Photon-Induced Reactions of Aromatics Adsorbed on Rough and Smooth Silver Surfaces

K. B. Myli, S. R. Coon, and V. H. Grassian*

Department of Chemistry, University of Iowa, Iowa City, Iowa 52242

Received: June 27, 1995[⊗]

We have investigated the thermal and photon-induced chemistry of several aromatics adsorbed on smooth and roughened Ag(111) surfaces at low temperatures (110 K). Pyrazine, pyridine, 3-chloropyridine, and chlorobenzene quantitatively desorb from Ag(111) near 200 K. After roughening the surface with 2 kV Ar ion bombardment, the breadth of the molecular desorption curves increases, and there is a high-temperature tail due to desorption from defect sites produced by the roughening process. Upon UV photolysis of 1 monolayer, chlorobenzene and 3-chloropyridine photodissociate on smooth and rough Ag surfaces, whereas no detectable photoreactions were observed for pyrazine or pyridine adsorbed on either surface. For the molecules that did undergo photodissociation, a shift to lower energy in the photodissociation threshold was observed on the rough surface relative to the smooth: 3.3 eV versus 3.5 eV for chlorobenzene and 3.5 eV versus 3.9 eV for 3-chloropyridine. We postulate that the decrease in the photodissociation threshold is due to defect sites produced by surface roughening, through either excitation of the surface plasmon resonance, which is allowed on the rough but not the smooth surface, or a more localized excitation near defect sites. Excitation in the molecular absorption band shows that the photodissociation yield is enhanced for 3-chloropyridine and quenched for chlorobenzene on the rough surface relative to the smooth. Theoretical calculations suggest that there is a decrease in the decay rate for 3-chloropyridine and an increase in the decay rate for chlorobenzene on the rough surface compared to the smooth. Differences between the quenching rates for 3-chloropyridine and chlorobenzene may be related to the different molecular orientations of these two molecules on the surface.

Introduction

The chemistry that occurs at defect sites is extremely important in catalysis and for surface reactions in general.[1] With the widespread use of scanning tunneling microscopy, it is evident there are a number of defect sites on atomically flat single crystal metal surfaces that are prepared by standard polishing techniques.[2] The consequences of defect sites are dependent on the detailed nature of the potential at that site. For example, metal surface atoms with low coordination number can be more reactive than those with higher coordination number.[3] As noted by Jenks et al., there can be cage effects involving defect sites resulting in slower reaction kinetics.[4] For some metals, defects produced by surface roughening cause enhanced optical properties including surface-enhanced Raman scattering (SERS)[5] and enhancements of 10^4 in second harmonic generation.[6]

The role of surface morphology, in particular surface roughness, on surface photochemistry has been the subject of a few theoretical and experimental studies. The discovery of surface-enhanced Raman scattering and the importance of surface morphology in SERS[5] prompted theoretical studies concerning the role of surface roughness on surface photochemistry.[7−9] Nitzan and Brus have modeled rough surfaces as isolated microscopic spheres protruding from the surface.[7] Their calculations predict an enhancement in the photochemical yield due to an increase in the molecular absorption cross section on a rough surface. The enhancement factor, defined as the absorption cross section of the adsorbed molecule relative to the free molecule, was calculated to be approximately 10−100, several orders of magnitude smaller than for SERS cross sections. There have been some reports in the literature of enhanced absorption for molecules adsorbed on Ag films.[10,11]

In a more recent study, Das et al. also predicted an enhancement in the photodissociation cross section for molecules adsorbed on a rough surface.[9] In their calculations, the rough surface was modeled as a hemispheroidal protrusion on a semiinfinite flat plane. The enhancement factor was found to depend on particle size and shape, as well as the distance of the molecule from the surface.

There have been a few experimental studies on the photochemistry of molecules adsorbed on rough metal surfaces. Using a focused CW Ar ion laser, Goncher et al. monitored the growth of surface graphite as a function of laser power and wavelength for a series of aromatics at and near a rough silver surface.[12] An enhanced two-photon process was proposed for the photodecomposition of benzene, pyridine, pyrazine, aniline, and acetophenone at 3.0 eV. Similar studies by Wolkow and Moskovitz have also shown enhanced multiphoton photochemistry on rough silver surfaces.[13] Franzke and Wokaun found a 10-fold enhancement in the decomposition of (2-methoxyphenyl)azosulfonate adsorbed on Ag island films as compared to in aqueous solution.[14] In contrast, other experiments found the rate of photochemical degradation of rhodamine 6G was greatly reduced on a rough silver surface.[15]

In related experiments on metal particles, Suh et al. determined that a two-photon process initiated the decomposition of 2-pyrazinecarboxylic acid adsorbed on colloidal silver.[16] A CW Ar ion laser was used for photolysis and as a SERS probe to measure the growth of graphitic carbon as a function of laser power and wavelength. Chen and Osgood examined the photodecomposition of dimethylcadmium adsorbed on cadmium particles with 4.8 eV photons by monitoring the growth of the Cd particles. They found evidence for structured particle growth which was related to the anisotropic electric field intensity around the particle.[17] Henglein and co-workers have examined

* To whom correspondence should be addressed.

[⊗] Abstract published in *Advance ACS Abstracts*, October 15, 1995.

0022-3654/95/2099-16407$09.00/0

reactions involving electron transfer from irradiated colloidal metal particles.[18-20]

Although surface-enhanced photochemistry is a topic that was addressed in the literature many years ago, there is a significantly greater understanding of surface photoprocesses since that time. The importance of substrate-mediated processes, previously neglected as a mechanism for surface photochemistry, has been demonstrated for many if not most surface photoreactions. Given the increased understanding of photon-induced processes at metal surfaces in the past several years, we felt that it would be informative to investigate the effect of surface roughness on surface photochemistry.

In this work we have investigated the role of surface morphology, in particular surface roughness, on the surface photochemistry of pyrazine, pyridine, 3-chloropyridine, and chlorobenzene adsorbed on smooth and rough Ag surfaces. The aromatics studied were chosen for several reasons. First, there have been two reports in the literature on enhanced photochemistry of pyrazine and pyridine adsorbed on rough silver surfaces.[12,13] Second, the photochemistry of chlorinated hydrocarbons on single crystal surfaces and the importance of substrate-mediated photochemistry for these molecules have been well documented in the literature.[21] Silver was chosen as a substrate because of its sharp, low plasmon frequency, making it the best optical enhancing substrate found thus far. The smooth surface, an atomically flat Ag(111) surface, is prepared by standard polishing techniques while the rough surface is prepared by ion sputtering the same surface. This method of sample preparation allows for the direct comparison of the effect of surface roughness on the same sample.

It is found that, under the conditions of this study, detectable photochemistry is only observed for chlorobenzene and 3-chloropyridine. In both of these molecules, the C−Cl bond photodissociates to give adsorbed phenyl or pyridyl groups and coadsorbed Cl atoms. As discussed in a preliminary report,[22] the photodissociation thresholds of these molecules are red-shifted from the gas phase, and the threshold on the rough surface is red-shifted from that on the smooth surface. In this paper, we characterize the adsorption of aromatics on rough and smooth silver surfaces by temperature-programmed desorption (TPD) and reflection absorption infrared spectroscopy (RAIRS) and measure the wavelength dependence of the chlorobenzene and 3-chloropyridine photoyields on the rough versus the smooth surface. We find that the photodissociation of chlorobenzene is somewhat quenched by surface roughness, whereas the photodissociation of 3-chloropyridine is enhanced. The results are discussed in terms of classical electromagnetic theory and the role of energy transfer and molecular orientation in these systems.

Experimental Section

Two ultrahigh-vacuum (UHV) chambers were used in these experiments. The first chamber has been previously described.[22] Briefly, the chamber is equipped with a cylindrical mirror analyzer (CMA), a quadrupole mass spectrometer (QMS), an ion sputter gun, and three gas dosers. The Auger electron and mass spectrometers are interfaced to a PC for data acquisition and analysis. Five mass signals can be monitored simultaneously in TPD. The Ag crystal is mounted in a tantalum cup that can be cooled with liquid nitrogen to 110 K. The tantalum cup is resistively heated and in direct contact with the crystal. The power supply used to heat the sample is interfaced to a PC, providing a linear temperature ramp from 110 to 900 K. Heating rates of 1.5 K/s are typically used for TPD. The temperature of the Ag sample is measured with a chromel−alumel thermocouple wire inserted into a small hole drilled near the edge of the crystal. The sample holder is held by a precision translation stage and a differentially pumped rotary drive.

RAIRS measurements were obtained by focusing the infrared light from a Mattson Galaxy 6021 Fourier transform infrared spectrometer onto the Ag crystal at grazing incidence (approximately 84° from the surface normal). The reflected beam was then focused onto a liquid nitrogen-cooled external MCT detector. The infrared beam entered and exited the chamber through BaF_2 windows. Unless otherwise noted, the RAIR spectra were acquired by averaging 1000 scans at an instrument resolution of 4 cm^{-1}.

The second UHV chamber is equipped with a scanning Auger microprobe and ion sputter gun. The chamber also has a vacuum transfer mechanism for quick sample introduction and removal. This second chamber was primarily used to prepare samples for surface characterization with scanning tunneling and atomic force microscopy, as discussed in the next section.

Two Ag(111) crystals were used in this study. Both were purchased from Monocrystals Inc. The samples were polished with alumina. The final steps of the polishing procedure included the use of 0.05 μm alumina followed by a colloidal silica suspension (Buehler). The sample was then heated under vacuum to 850 K and removed for a final polish with the colloidal silica suspension.

Ag(111) is cleaned by 2 kV Ar^+ bombardment to remove sulfur and oxygen impurities from the surface. A smooth surface is prepared by subsequent annealing of the sample to 800 K. A rough surface is prepared by 2 kV Ar^+ sputtering at room temperature for several (2−4) hours. This procedure has been shown to give a Ag surface that exhibits SERS.[12]

$C_4H_4N_2$, C_5H_5N, C_6H_5Cl, and 3-C_5H_4ClN were purchased from Aldrich and freeze−pump−thawed several times prior to use. Gases are introduced by backfilling the chamber, and gas exposures are given in units of langmuir, where 1 langmuir = 1×10^{-6} Torr s. One monolayer (ML) coverages were prepared by exposing the surface to enough gas to adsorb multilayers. The sample was then heated to just past the multilayer desorption peak and cooled back down.

The third harmonic of a 10 Hz Nd:YAG laser (Continuum YG661-10) and the frequency-doubled light from a Nd:YAG pumped dye laser (Continuum TDL-60) were used to photolyze the sample at various photon energies. The laser beam irradiated the sample at an angle of 30° with respect to the surface normal. Photolysis times of 2 h were typical, and the laser fluence was kept below 10 mJ/cm^2 per pulse in order to minimize thermal effects. In addition, the sample was biased −90 V during photolysis to eliminate electron beam induced chemistry from stray electrons in the vacuum chamber.

Results and Discussion

1. Characterization of Surface Roughness. Both scanning tunneling microscopy (STM) and atomic force microscopy (AFM) were used to examine the degree of surface roughness and to probe the types of defect sites that may be present on the surface after sputtering. The surface was sputtered with 2 kV Ar^+ for several hours at approximately 40° from the surface normal. Images were obtained in air within 2−3 h after removal from the UHV chamber.

The sputtered surface exhibits large bumps and pits in the range of 75 nm in diameter. The most notable structures of the surface were large, irregularly shaped bumps and elliptical pits. The in-plane dimensions of these structures were on the order of hundreds of nanometers. In contrast, the height of the structures was generally less than 20 nm. Smaller features on the order of tens of nanometers (in-plane) by less than 1 nm (vertical) were superimposed on the larger structures. This

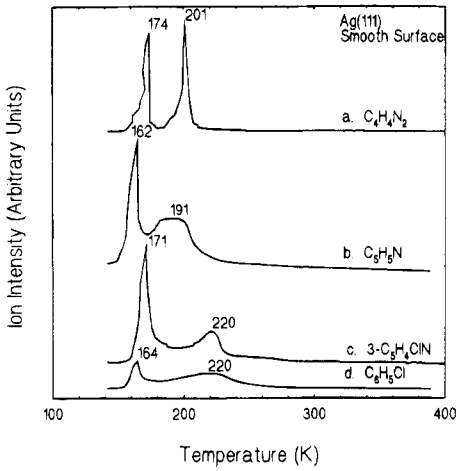

Figure 1. Molecular desorption of several aromatics from a smooth Ag(111) surface are shown following adsorption at $T = 110$ K: (a) $C_4H_4N_2$, (b) C_5H_5N, (c) 3-C_5H_4ClN, and (d) C_6H_5Cl.

nanostructured topography is thought to be responsible for most of the enhancement in SERS.[23] Smaller features are present on the roughened surface and represent sites of low coordination number.

2. TPD of $C_4H_4N_2$, C_5H_5N, 3-C_5H_4ClN, and C_6H_5Cl Adsorbed on Ag(111). TPD spectra were obtained for $C_4H_4N_2$ ($m/e = 80$), C_5H_5N ($m/e = 79$), 3-C_5H_4ClN ($m/e = 113$), and C_6H_5Cl ($m/e = 112$) from a smooth Ag(111) surface following adsorption at $T = 110$ K. The high-exposure data (3.0 langmuirs for $C_4H_4N_2$, C_5H_5N, and 3-C_5H_4ClN and 5.0 langmuirs for C_6H_5Cl) are presented in Figure 1. $C_4H_4N_2$ desorbs with a desorption rate maximum (T_{max}) of 201 K at low exposures. As the exposure is increased above 1 langmuir, the peak at 201 K saturates, and a second peak grows in at lower temperatures with a T_{max} of 174 K (Figure 1a). The low-temperature peak is assigned to desorption of multilayers, and the high-temperature peak is assigned to desorption of the monolayer. We do observe peaks in TPD for several other ions including $C_2H_2^+$ ($m/e = 26$) and HCN^+ ($m/e = 27$); however, the peak shape and temperature maxima for these ions were identical to the molecular ion peak, $C_4H_4N_2^+$ ($m/e = 80$), and, therefore, are attributed to fragments of the parent ion.

C_5H_5N quantitatively desorbs from the surface with a $T_{max} = 191$ K at low exposures. This peak does saturate as a function of gas exposure and has been assigned to monolayer desorption. A second peak grows in at exposures above 1 langmuir with a T_{max} of 162 K. This second feature does not saturate with increasing exposure and is assigned to multilayer desorption. The TPD spectrum for this molecule is shown in Figure 1b. No other desorption peaks except for fragments of the parent ion were detected in TPD.

TPD studies of 3-C_5H_4ClN and C_6H_5Cl yielded similar results. Two desorption peaks are present in TPD (Figure 1c,d): a high-temperature peak that saturates with increasing exposure and a low-temperature peak that does not. Accordingly, the high-temperature peak is assigned to desorption of the monolayer, and the low-temperature peak is assigned to multilayer desorption. For 3-C_5H_4ClN the desorption rate maximum temperatures for multilayer and monolayer desorption are near 171 and 220 K, respectively. The T_{max} for monolayer desorption of C_6H_5Cl monolayers is near 220 K, and the mulitlayer desorbs near 164 K. No evidence for the desorption of $AgCl^+$ ($m/e = 142$) or products formed from coupling reactions, i.e., biaryls, was seen.

We can calculate the activation energy of desorption for pyrazine, pyridine, 3-chloropyridine, and chlorobenzene from Ag(111) using the data presented in Figure 1.[24] The monolayer desorption rate maxima are at 201, 191, 220, and 220 K for pyrazine, pyridine, 3-chloropyridine, and chlorobenzene, respectively, were used to calculate monolayer desorption energies.[25] Activation energies for monolayer desorption are given in Table 1. The activation energies for desorption of the multilayer were calculated using the leading edge method of analysis.[26] The multilayer desorption energies are also given in Table 1. When known, the value of the multilayer desorption energy is in good agreement with the heat of sublimation.[27]

TABLE 1: Activation Energies of Desorption (in kJ/mol) for $C_4H_4N_2$, C_5H_5N, 3-C_5H_4ClN, and C_6H_5Cl Adsorbed on Ag(111)

molecule	monolayer[a]	multilayer[b]
$C_4H_4N_2$	52	50
C_5H_5N	50	47
3-C_5H_4ClN	57	50
C_6H_5Cl	57	48

[a] The activation energies of desorption for monolayer desorption were calculated using the Redhead method of analysis for first-order desorption kinetics (ref 24). A preexponential factor of 1×10^{13} s^{-1} was used in the calculation. [b] The activation energies of desorption for multilayer desorption were calculated using the leading edge method of analysis (ref 26).

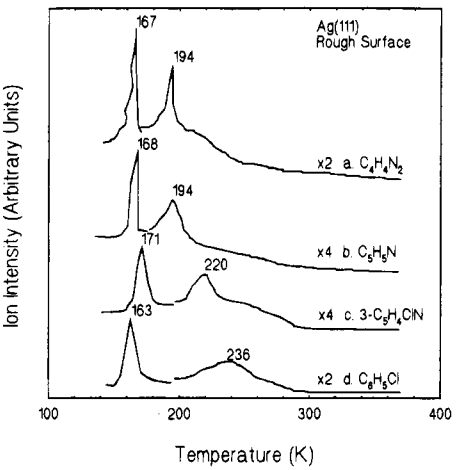

Figure 2. Molecular desorption from a roughened Ag(111) surface are shown following adsorption at $T = 110$ K: (a) $C_4H_4N_2$, (b) C_5H_5N, (c) 3-C_5H_4ClN, and (d) C_6H_5Cl.

3. TPD of $C_4H_4N_2$, C_5H_5N, 3-C_5H_4ClN, and C_6H_5Cl Adsorbed on Roughened Ag. The molecular desorption of $C_4H_4N_2$, C_5H_5N, 3-C_5H_4ClN, and C_6H_5Cl from a rough Ag surface following adsorption at $T = 110$ K was also studied. The shape of the multilayer desorption peak does not change with surface roughness, but the monolayer peak does change. It can be seen from the spectrum shown in Figure 2a that the shape of the $C_4H_4N_2$ ($m/e = 80$) monolayer desorption trace changes on the rough surface relative to the smooth. On the rough surface there is a high-temperature shoulder that extends to approximately 270 K. The magnitude of the high-temperature shoulder is dependent on the degree of surface roughness. We have found that the degree of surface roughness is altered when the sample is warmed well below the annealing temperature. Therefore, for the experiments done on the rough Ag surface, the sample was not heated after sputtering.

The TPD spectra following adsorption of C_5H_5N on a rough surface is shown in Figure 2b. A broad high-temperature shoulder is observed in TPD for monolayer desorption from the rough surface. For C_5H_5N, this tail extends out to 280 K. The desorption traces for HCN^+ ($m/e = 27$) and $C_2H_2^+$ ($m/e = 26$) (not shown) follow that for the molecular ion, $C_4H_5N^+$ ($m/e = 79$).

The desorption of the chlorinated aromatics 3-C_5H_4ClN and C_6H_5Cl from a rough Ag surface is also shown in Figure 2c,d. The molecular desorption curve shows a high-temperature shoulder for 3-C_5H_4ClN (see Figure 2c). The chlorobenzene molecular desorption curve is not as sharp as the desorption curves for $C_4H_4N_2$, C_5H_5N, or 3-C_5H_4ClN. The desorption trace for monolayer desorption of C_6H_5Cl from roughened Ag(111) is broader, and the desorption rate temperature maximum shifts to higher temperatures compared to desorption from smooth Ag(111) (Figure 1d). Besides the molecular peaks and the mass spectral fragments associated with those peaks, no other desorption products were detected in TPD after adsorption of 3-C_5H_4ClN and C_6H_5Cl on a rough Ag surface.

In general, for the four molecules investigated on the roughened Ag(111) surface, the multilayer desorption remains the same in terms of the peak shape; however, the monolayer desorption peak broadens and is much more asymmetric with a high-temperature shoulder. The broadening of the monolayer desorption peak on the rough surface can be related to an increase in the surface heterogeneity and therefore the density of defect sites with different desorption energies, thus causing a temperature spread in the desorption peak. The sharp feature in the desorption traces for $C_4H_4N_2$, and C_5H_5N, and 3-C_5H_4-ClN shows that there is still some desorption from 111 facets on the rough surface. Because there is no desorption occurring at the higher temperatures on the annealed Ag(111) sample (the smooth surface), we conclude that the molecules desorbing at higher temperatures are desorbing from defect sites produced by Ar ion bombardment.

There is only a modest increase in the surface area after roughening the surface. We can estimate the change in surface area by comparing the integrated areas of the desorption curves for the rough and smooth surfaces. Using the 3-chloropyridine TPD data, we calculate that the surface area increases by less than 5% upon roughening. The increase in surface area determined from STM images corroborate the TPD data and gave a modest increase in surface area on the rough surface, on the order of 2%.

4. RAIRS of C_6H_5Cl and 3-C_5H_4ClN Adsorbed on Ag(111). The adsorbate orientation of pyrazine and pyridine on Ag(111) has been determined by electron energy loss spectroscopy (EELS).[28-30] Pyrazine lies flat with its molecular plane parallel to the surface at all coverages. Pyridine undergoes a change in orientation from flat to tilted as the coverage increases. The orientation of chlorobenzene on Ag(111) has been determined to be flat based on EELS and X-ray photoelectron spectroscopy.[31,32] We have used RAIRS to determine the orientation of chlorobenzene and 3-chloropyridine at high coverages on smooth Ag(111). Figure 3 shows RAIRS data for a 30 langmuir exposure of chlorobenzene adsorbed on Ag(111) at 110 K. The multilayer RAIR spectrum (Figure 3a) shows several bands in the spectral region extending from 900 to 1600 cm^{-1}. The peak at 908 cm^{-1} is assigned to the out-of-plane C−H deformation mode. The peaks at 1003, 1023, 1069, 1085, and 1123 cm^{-1} are assigned to in-plane C−H deformation modes. These four peaks are assigned to the ring carbon−carbon stretching mode, 1446, 1479, 1570, and 1584 cm^{-1}. A peak at 3071 cm^{-1} (not shown in Figure 3) is assigned to the symmetric C−H stretching mode. Figure 3b shows the RAIR spectra after the sample was heated to 180 K to remove the multilayer. A monolayer of chlorobenzene results in no observable infrared peaks in the spectrum. This is consistent with the EELS data of chlorobenzene adsorbed on Ag(111) studied by Song et al.[31] The EEL spectrum of chlorobenzene shows three losses at 470, 740, and 3050 cm^{-1} for monolayer adsorption recorded in the specular direction. On the basis of

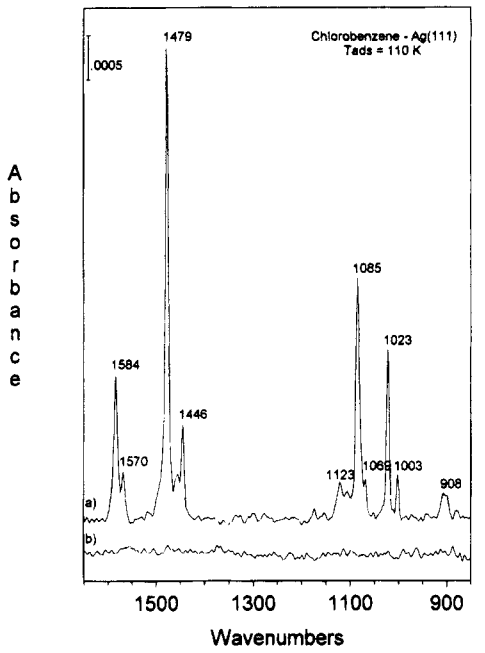

Figure 3. FTIR spectra are shown of (a) multilayers of chlorobenzene (30.0 langmuirs) adsorbed on Ag(111) at approximately 110 K (b) and after heating to 180 K. The sample was cooled back to 110 K before each spectrum was recorded.

off-specular measurements and the absence of many of the in-plane modes in the spectrum recorded in the specular direction, Song et al. concluded that chlorobenzene is oriented with the aromatic ring plane parallel to the surface.[31] The bands at 470 and 740 cm^{-1} are outside the spectral range of our instrument, and although the band at 3050 cm^{-1} is accessible for spectroscopic detection, its intensity is primarily due to impact scattering and therefore would not be detected with reflectance IR spectroscopy. Using the EELS and the RAIRS results along with the surface selection rule, it can be concluded that chemisorbed chlorobenzene lies flat on the surface with its ring plane parallel to the surface plane.

Figure 4 shows RAIRS data for 3-chloropyridine adsorbed on Ag(111) at approximately 110 K. The peak at 804 cm^{-1} is assigned to the out-of-plane C−H deformation mode. The peaks at 1019, 1035, 1096, and 1110 cm^{-1} are assigned to the in-plane C−H deformation mode. The ring C−C stretching modes are assigned to two intense peaks at 1417 and 1469 cm^{-1}. The peaks at 1564 and 1574 cm^{-1} are assigned to the interaction between ring C=C and C=N stretching vibrations. The symmetric C−H stretching mode is assigned to a peak at 3048 cm^{-1} (not shown in Figure 4). Figure 4b shows spectra after heating to 195 K to remove the multilayer, resulting in the disappearance of the peaks at 804 and 3048 cm^{-1}, and the remaining peaks decrease considerably in intensity and shift by less than 5 cm^{-1}. Warming the sample past the monolayer desorption peak results in the disappearance of all IR peaks in the spectrum (Figure 4c). The peaks at 1019, 1469, 1574, and 3048 cm^{-1} are very close in frequency to the frequencies observed in HREELS for one monolayer of pyridine adsorbed on Ag(111).[28-30] From the EELS data, it has been determined that pyridine bonds through the nitrogen lone pair at high coverages on Ag(111) with an estimated tilt of 35° with respect to the surface normal. Therefore, the similarities between frequencies for adsorbed pyridine at high coverages and for 3-chloropyridine at high coverages suggest a tilted orientation with the nitrogen lone pair bonded to the surface for 3-chloropyridine.

From the absence of peaks in the RAIR spectrum recorded for 1 ML of chlorobenzene and the presence of peaks due to

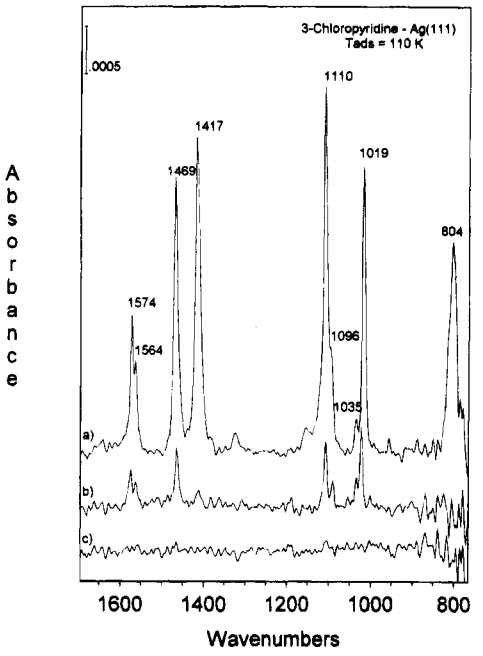

Figure 4. FTIR spectra are shown of (a) multilayers of 3-chloropyridine (30.0 langmuirs) adsorbed on Ag(111) at approximately 110 K and after heating (b) to 195 K and (c) 230 K. The sample was cooled back to 110 K before each spectrum was recorded.

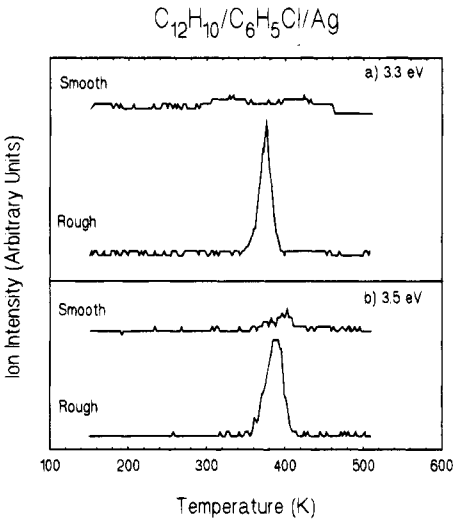

Figure 5. (a) Biphenyl (amu = 154) is detected in TPD from roughened Ag(111) but not from a smooth Ag(111) surface after excitation of 1 ML of adsorbed chlorobenzene with 3.3 eV photons. (b) Biphenyl (amu = 154) is detected in TPD from smooth and roughened Ag(111) after excitation of 1 ML of adsorbed chlorobenzene with 3.5 eV photons. Biphenyl was not detected in TPD from either surface after excitation of 1 ML of adsorbed chlorobenzene with 3.1 eV photons.

in-plane modes in the RAIR spectrum recorded for 1 ML of 3-chloropyridine, it can be concluded that these molecules bond to Ag(111) with different adsorbate orientations. The RAIRS data for chlorobenzene are consistent with the XPS and EELS data for this molecule. All three techniques provide evidence for a flat bonded orientation for chlorobenzene with the aromatic ring plane parallel to the surface, similar to the adsorbate orientation for benzene on Ag(111).[29] The high-coverage RAIRS data for 3-chloropyridine are similar to the high-coverage EELS data for pyridine on Ag(111)[28-30] and provide evidence for a tilted orientation for 3-chloropyridine with the nitrogen end of the molecule bonded to the surface.

5. Surface Photochemistry of $C_4H_4N_2$, C_5H_5N, 3-C_5H_4ClN, and C_6H_5Cl Adsorbed on Smooth and Roughened Ag(111). There were no photoproducts detected in TPD after UV photolysis of 1 ML of $C_4H_4N_2$ and C_5H_5N adsorbed on smooth or roughened Ag(111). Several photon energies were used for excitation including 5.6, 5.0, 4.7, 4.4, and 3.1 eV. Besides as fragments of the parent molecular ion, the following ions were monitored but did not exhibit any additional features in TPD: H_2 (m/e = 2), C_2H_2 (m/e = 26), HCN (m/e = 27), and C_2N_2 (m/e = 52).

Although our results initially appear to be in contrast to those of Goncher et al.[12] and Wolkow and Moskovits,[13] a close comparison of the experiments reveals that this is not necessarily true. In those experiments, decomposition of pyridine[12] and pyrazine[12,13] on rough silver surfaces was monitored by the increase of graphite features in SERS. Both studies indicate that a two-photon process is the rate-limiting step for decomposition to graphite. The power density (photons/cm^2 s) in our experiments was at least as high as the highest power density employed in those experiments. Thus, graphite formation should have occurred at the same rate in our experiment, if the systems were otherwise equivalent. That we see no evidence of *any* photodecomposition, let alone decomposition to graphite, is most likely due to the fact that we adsorbed only 1 ML of pyridine or pyrazine on the rough silver surface. Both Goncher et al. and Wolkow and Moskovits observed very little decomposition from a single monolayer. The decomposition rate increased as a function of coverage and reached a maximum when many layers of the molecules were adsorbed. As the coverage was increased further, the rate decreased again. Wolkow and Moskovits model this behavior as a tuning of the surface plasmon resonance as a function of the thickness of a dielectric coating of adsorbed molecules on surface roughness features. This tuning effect depends on the wavelength of light, the size of the roughness features, and their shape and density, as well as on the thickness of the coating layer. Enhancements in the photodecomposition rate of several orders of magnitude are predicted by the model for coating thicknesses corresponding to many molecular layers. Only a small enhancement is predicted for a single monolayer; thus, the rate of photodecomposition for these molecules under the experimental conditions used in this study may be too small to be detected.

Although no photoproducts were detected for pyrazine or pyridine, UV photolysis of 1 ML of 3-chloropyridine and chlorobenzene adsorbed on smooth and roughened Ag(111) resulted in C−Cl bond dissociation. Bipyridyl and biphenyl desorb in postirradiation temperature-programmed desorption after UV excitation of 3-chloropyridine and chlorobenzene, respectively. AgCl is also detected in TPD near 800 K. Although similar photoproducts are formed on the rough and smooth surface, there is a red shift in the photodissociation threshold of chlorobenzene and 3-chloropyridine when adsorbed on a rough silver surface as compared to a smooth surface. Figure 5 shows the temperature-programmed desorption data after photolysis of chlorobenzene on a smooth and rough surface at two wavelengths. Figure 5a shows the desorption trace of biphenyl (m/e = 154) after excitation of chlorobenzene with 3.3 eV photons followed by heating. A peak is observed near 400 K for the rough surface but not the smooth one. A peak near 400 K in the biphenyl desorption trace is present on both surfaces after excitation with 3.5 eV photons (see Figure 5b). Biphenyl desorption is not detected in TPD after photolysis with 3.1 eV photons on either a rough or smooth surface. The photodissociation thresholds on both surfaces are red-shifted from that of the gas phase[33] (see Table 2), and the rough surface has a lower energy threshold than the smooth.

Similar shifts are observed for the photolysis of adsorbed 3-chloropyridine. Bipyridyl (m/e = 156) is detected in TPD after excitation of 3-C_5H_4ClN with 3.5 eV photons when

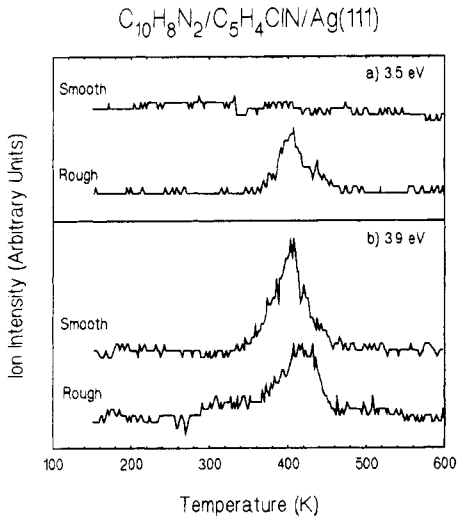

Figure 6. (a) Bipyridyl (amu = 156) is detected in TPD from roughened Ag(111) but not from a smooth Ag(111) surface after excitation of 1 ML of adsorbed 3-chloropyridine with 3.5 eV photons. (b) Bipyridyl (amu = 156) is detected in TPD from smooth and roughened Ag(111) after excitation of 1 ML of adsorbed 3-chloropyridine with 3.9 eV photons. Bipyridyl was not detected in TPD from either surface after excitation of 1 ML of adsorbed 3-chloropyridine with 3.3 eV photons.

TABLE 2: Photodissociation Thresholds (in eV) for 1 ML of Adsorbed Chlorobenzene and 3-Chloropyridine

molecule	photodissociation threshold	adsorbed vs gas phase
C_6H_5Cl	3.9	gas phase[a]
	3.5	Ag(111)
	3.3	roughened Ag(111)
3-C_5H_4ClN	4.1	gas phase[b]
	3.9	Ag(111)
	3.5	roughened Ag(111)

[a] Reference 33. [b] Estimated from the absorption cross section.

adsorbed on the rough surface but not on the smooth surface (Figure 6a). Excitation of 3-C_5H_4ClN with 3.9 eV photons results in the formation of bipyridyl on both surfaces (Figure 6b). Bipyridyl desorption is not detected in TPD after photolysis with 3.3 eV photons on either surface. The measured threshold values for 3-C_5H_4ClN are shown in Table 2.

One possible explanation for the longer wavelength threshold on the rough surface is due to excitation of a surface plasmon resonance which is only allowed on rough surfaces. Although both p- and s-polarized light can couple to surface plasmon resonances on rough surfaces, p-polarized light does so more effectively. We have measured the effect of polarization on the photodissociation yield of 3-chloropyridine. The yield increases by a factor of 2.3 when p-polarized light is used at an incident angle of 30°. This compares well with a value of 3.6 obtained from photoemission studies at an incident angle of 22.5°.[35]

Castro and White have previously discussed how excitation of a delocalized plasmon resonance could lead to photodesorption of SO_2 from Ag(111).[36] The delocalized excitation can relax into single particle states, which then couple to the adsorbate. For SO_2, this coupling results in desorption, but for 3-chloropyridine and chlorobenzene, it results in C−Cl bond dissociation.

Another possible explanation for the threshold shift that cannot be entirely ruled out is one that involves a more localized excitation of the surface−adsorbate complex at defect sites. Before the exact mechanism for the threshold lowering is determined, more information about the local electronic structure and work function at defect sites relative to the adsorbate energy levels would be needed.

TABLE 3: Ratio of the Photoyields, Y_R/Y_S, Measured at Several Photon Energies for 1 ML of Adsorbed 3-Chloropyridine and Chlorobenzene

photon energy (eV)	Y_R/Y_S[a]
3-chloropyridine	
4.0	1.2
4.4	1.2
4.7	3.1
5.0	3.6
5.6	6.6
chlorobenzene	
3.9	0.2
4.4	0.7
5.0	0.8

[a] For 3-chloropyridine Y_R/Y_S = [(TPD yield for $C_{10}H_8N_2)_{rough}$]/[(TPD yield for $C_{10}H_8N_2)_{smooth}$]. For chlorobenzene, Y_R/Y_S = [(TPD yield for $C_{12}H_{10})_{rough}$]/[(TPD yield for $C_{12}H_{10})_{smooth}$]. Based on several measurements at each photon energy, the error in the ratio Y_R/Y_S is estmated to be approximately 25%.

Photolysis at higher photon energies results in approximately a 100-fold increase in the photoyield for both 3-chloropyridine and chlorobenzene. At approximately 3.9 eV and above, both molecules absorb light.[34] At 5 eV, the photodissociation cross section determined from the TPD data for 1 ML of 3-chloropyridine and chlorobenzene adsorbed on Ag(111) were approximately the same: $(2.0 \pm 0.2) \times 10^{-21}$ and $(2.5 \pm 0.2) \times 10^{-21}$ cm^2, respectively. In order to determine whether there was an enhancement in the dissociation yield on the rough surface relative to the smooth at the higher photon energies, we have measured the relative yield of bipyridyl and biphenyl formation on both surfaces from photolysis of 1 ML of 3-chloropyridine and chlorobenzene, respectively. The ratio of the photodissociation yields, Y_R/Y_S, was determined by taking the integrated areas of the TPD curves for the photoproducts. The ratio Y_R/Y_S for 3-chloropyridine and chlorobenzene on rough and smooth surfaces at several photon energies is given in Table 3. For 3-chloropyridine, there is a slight enhancement of 1.2 for excitation on the rough surface at 4.0 eV and a larger enhancement of 6.6 at 5.6 eV. For chlorobenzene, the photolysis is quenched on the rough surface relative to the smooth; i.e., $Y_R/Y_S < 1$ at all photon energies studied. The ratio Y_R/Y_S increases as a function of photon energy for both molecules.

In order to gain more insight into the cause of the enhanced photochemistry of 3-chloropyridine and quenched photochemistry of chlorobenzene on the rough surface, we have modeled the absorption cross section of these two molecules. The basis of the theory and some of the theoretical results are described below.

6. Theoretical Model. Enhanced photochemical yields of molecules on rough metallic surfaces were modeled by Nitzan and Brus using classical electromagnetic theory.[7] In the model, the molecule is represented by a classical point dipole characterized by a static polarization, α_m, resonance frequency, w_m, and decay rate, Γ. The surface is modeled as an isolated microscopic sphere and characterized by a dielectric function

$$\epsilon(\omega) = \epsilon_1(\omega) + i\epsilon_2(\omega) \quad (1)$$

There are several restrictions placed on the system in order to simplify the calculations. First, the sphere must be smaller than the wavelength of the incident light. Second, the molecule is taken to lie on the z axis (with the sphere center at the origin), and the induced molecular dipole is taken to be perpendicular to the surface. Third, the substrate is assumed to behave as a Drude-like free electron metal.

Using the model of Nitzan and Brus,[7] the absorption cross section for the adsorbed molecule can be calculated from eq 2,

$$\sigma_{ab}(\omega) = \frac{4\pi}{3}\frac{\omega}{c}\,\mathrm{Im}[D_1(\omega)\,D_3(-\omega) + D_2(\omega)\,D_4(-\omega)] \qquad (2)$$

where

$$D_1(\omega) = \alpha_m \frac{\omega_m^2[2\omega_s^2\alpha_s/R^3 + B(\omega)]\cos\theta_m}{A(\omega)\,B(\omega) - \omega_m^2\omega_s^2(\alpha_m\alpha_s/R^6)(3\cos^2\theta_m + 1)} \qquad (2a)$$

$$D_2(\omega) = \alpha_m \frac{\omega_m^2[-\omega_s^2\alpha_s/R^3 + B(\omega)]\sin\theta_m}{A(\omega)\,B(\omega) - \omega_m^2\alpha_s^2(\alpha_m\alpha_s/R^6)(3\cos^2\theta_m + 1)} \qquad (2b)$$

$$D_3(\omega) = \cos\theta_m + \frac{\omega_s^2\alpha_s}{B(\omega)R^3}\left(\frac{D_1(\omega)}{R^3}(3\cos^2\theta_m + 1) + 2\cos\theta_m\right) \qquad (2c)$$

$$D_4(\omega) = \sin\theta_m + \frac{\omega_s^2\alpha_s}{B(\omega)R^3}\left(\frac{D_2(\omega)}{R^3}(3\cos^2\theta_m + 1) + \sin\theta_m\right) \qquad (2d)$$

$$A(\omega) = \omega_m^2 - \omega^2 - i\omega\Gamma \qquad (2e)$$

$$B(\omega) = (\omega_s^2 + \gamma^2/4) - \omega^2 - i\omega\gamma \qquad (2f)$$

In the above equations c is the speed of light, R is the distance from the center of the sphere to the center of the molecule ($R = d + a$, where d is the molecule−surface distance and a is the sphere radius), θ_m is the angle of the molecule with respect to the surface normal, α_m is the static molecule polarizability, α_s is the apparent static sphere polarizability, ω_s is the sphere resonance frequency, ω_m is the molecule resonance frequency, ω is the frequency of the photon, γ is the width of the dipole resonance, and Γ is the molecular decay rate. The width of the dipole resonance is calculated using eq 3,

$$\gamma = (2\epsilon_2(\omega)/\epsilon'_1(\omega))_{\omega=\omega_s} \qquad (3)$$

where

$$\epsilon'_1(\omega) = d\epsilon_1(\omega)/d\omega \qquad (3a)$$

This simple model has neglected the interaction between the spheres and assumes that all the spheres on the surface have the same shape corresponding to the same frequency. This would not be true in our experiments, because that kind of surface roughness uniformity would be impossible with our method of sample preparation. Therefore, our experimental data would be a combined result of excitation of "spheres" of different shapes with different frequencies. Nevertheless, we have calculated the absorption cross sections using this classical model and will consider the model in light of the experimental data.

We have used the constants given in ref 7 for the Ag substrate. The parameters for the molecular frequencies, 4.68 eV (37740 cm^{-1}) and 4.70 eV (37879 cm^{-1}),[34] and the static molecular polarizabilities, 11.5×10^{-24} and 13.2×10^{-24} cm^3,[37] were used for 3-chloropyridine and chlorobenzene, respectively. We have investigated the effect of three parameters on the shape and intensity of the absorption cross section. These three parameters are the decay rate, Γ, the sphere radius, a, and the molecule−surface distance, d.

As seen in Figure 7a, the decay rate has a significant effect on the shape of the absorption cross section as a function of photon energy and on whether there is enhanced absorption. Figure 7a shows there is a change in the relative intensities of the Ag resonance, 3.5 eV (28 230 cm^{-1}), and the molecular resonance, 4.68 eV (37 740 cm^{-1}). As the molecular decay rate is increased, the molecular resonance decreases until it is no longer visible on this scale, and the sphere resonance grows in intensity. This is due to the competition between two processes: the transfer of energy from the radiative particle modes to the molecule and the damping of molecular energy due to transfer into the nonradiative particles modes.

The effect of the sphere radius on the shape and intensity of the absorption cross section is shown in Figure 7b. The smaller the radius of the sphere, the more intense both the molecular and sphere absorptions. As the radius of the sphere is increased, both peaks decrease in intensity. This has to do with the fact that as the spheres become smaller, they become better radiators because they are able to develop large dipoles.[8]

Figure 7c shows the effect of molecule−surface distance. As the distance is increased, the sphere resonance decreases in intensity and the molecule resonance increases. As the distance from the surface becomes very large, i.e. 1000 nm, the possibility for interference between the molecule and the sphere dipoles is reduced, leading to a decrease in intensity of the Ag resonance and an increase in the molecule resonance. It should be noted that although the total integrated absorption cross section, sphere and molecular resonance, increases relative to the "free molecule" ($d \rightarrow \infty$), the integrated cross section of the molecular resonance decreases relative to the free molecule. This condition holds for molecules with $\omega_m > \omega_s$. Therefore, the number of effective photons, i.e., those that cause photochemistry, may be decreased for the adsorbed versus the free molecule.

7. Comparison between Experiment and Theory. Although the model described above was not intended to be used for smooth surfaces, we can try to extract the importance of the various parameters on the absorption cross section. It can be seen in Figure 7a that the absorption cross section depends strongly on the decay rate. In Figure 8, the integrated absorption cross section (integrated from 4.3 to 5.5 eV, corresponding to the molecular resonance) is plotted as a function of the decay rate. The theoretical results show there is a decrease in the absorption cross section as the molecular decay rate is increased for both molecules. Assuming that an enhanced or quenched absorption cross section results in an enhanced or quenched photodissociation yield, the results shown in Figure 8 predict that for an enhanced photodissociation yield for 3-chloropyridine on a rough surface, the decay rate for the smooth surface has to be larger than on the rough ($\Gamma_S > \Gamma_R$). The opposite trend ($\Gamma_S < \Gamma_R$) is needed to predict a quenched photodissociation yield for chlorobenzene adsorbed on a rough relative to a smooth surface.

The two different molecular orientations for 3-chloropyridine (tilted) and chlorobenzene (flat) may play a role in the decay rates and how the decay rates change on the rough versus the smooth surface. It has been proposed by Zhou and White[32] that the photodissociation of chlorobenzene adsorbed on Ag is partially due to substrate-mediated process, similar to that found for adsorbed CH_3Cl and C_2H_5Cl but with a lower cross section. The smaller cross section was attributed to the greater interaction between the surface and the flat π-bonded chlorobenzene as compared to the tilted halogen-bonded methyl chloride. Thus, the excited antibonding (σ^*) orbital of the chlorobenzene is

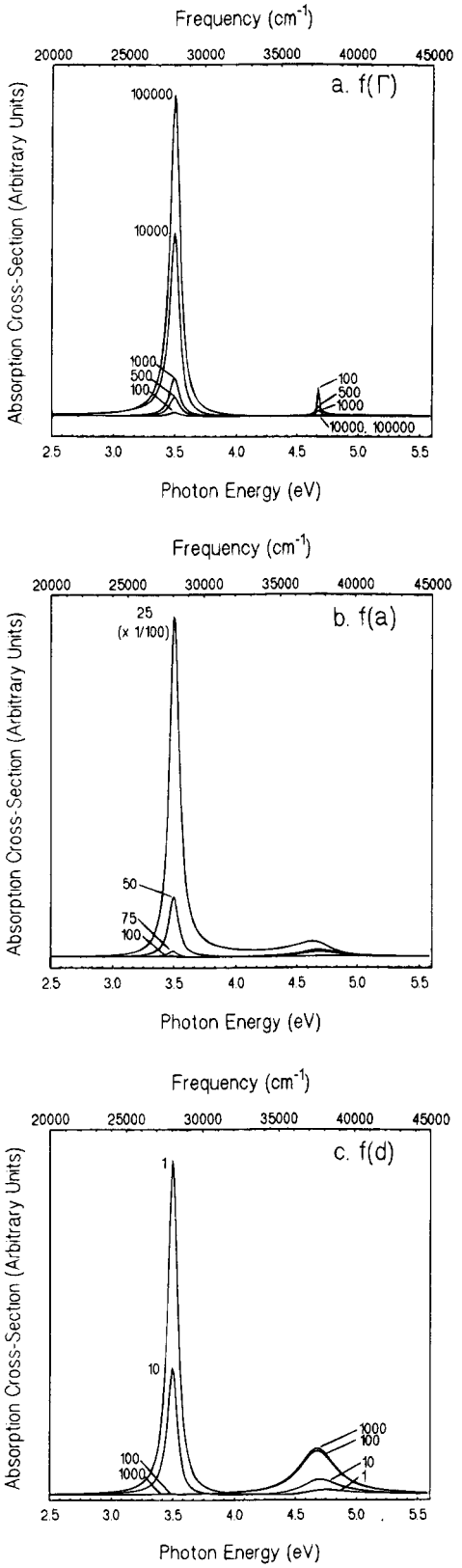

Figure 7. Effect of the different parameters on the calculated absorption cross section. The calculations were done using the parameters given in the text for silver and 3-chloropyridine; similar results were obtained for chlorobenzene. (a) Calculated absorption cross section as a function of the decay rate, Γ: Γ = 100, 500, 1000, 10 000, and 100 000 cm^{-1}. The sphere radius, a, and the molecule−surface distance, d, were constant at 1 nm and 50 nm, respectively. (b) Calculated absorption cross section as a function of the sphere radius, a: a = 25, 50, 75, and 100 nm. The decay rate, Γ, and the molecule−surface distance, d, were constant at 3000 cm^{-1} and 1 nm, respectively. (c) Calculated absorption cross section as a function of the the molecule−surface distance, d: d = 1, 10, 100, and 1000 nm. The decay rate, Γ, and the sphere radius, a, were constant at 3000 cm^{-1} and 50 nm, respectively.

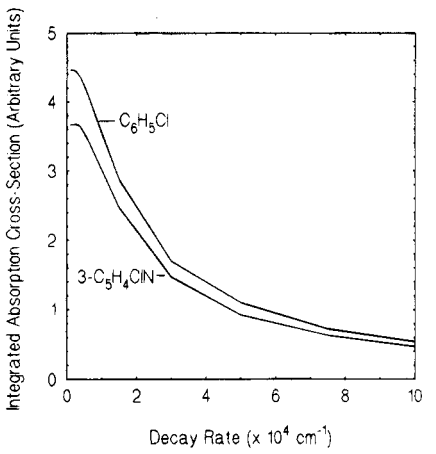

Figure 8. Calculated integrated absorption cross sections from 4.3 to 5.5 eV corresponding to the molecular resonance for 3-chloropyridine and chlorobenzene as a function of the decay rate.

closer to the surface and is quenched faster. The small random roughness model (SRRM) predicts that the energy transfer efficiency from the dipole to the rough surface is much larger than that of the smooth surface.[38] In addition, it is known that the C−C stretching modes of aromatics play a role in the excited-state decay processes.[39−41] Fischer and Schneider analyzed the time-dependent correlation function and found that approximately 34% of the energy goes into the totally symmetric skeletal breathing mode, C−C stretching mode, and, to a smaller extent, the out-of-plane vibrations.[39] Since chlorobenzene lies parallel to the surface, the energy deposited in its C−C bonds can readily be quenched due to the close proximity to the surface. The SRRM predicts that quenching of the energy deposited into the C−C bonds of chlorobenzene would be faster on the rough than the smooth surface, resulting in a lower photoyield on the rough surface. For 3-chloropyridine, the tilted geometry may favor enhanced absorption and reduced energy transfer to the substrate, thus giving rise to an enhanced photoyield.

Although we have used classical electromagnetic theory to model the results, its limitations were anticipated. Some of the results cannot be explained by the model, including the dependence of the photodissociation yield on photon energy. Also, it has been recently shown that classical electromagnetic theory does not accurately predict the distance dependence of some surface photochemical reactions at distances close to the surface.[42] Further development in theory is needed in order to understand the details of the results presented here.

Conclusions

There are several differences in the surface chemistry and photochemistry of pyrazine, pyridine, chlorobenzene, and 3-chloropyridine when adsorbed on a rough as compared to a smooth surface. A localized effect is evident in the temperature-programmed desorption curves; either the desorption maxima shift to higher temperatures, or there is a high-temperature desorption tail. There is also a modest increase in surface area as reflected in the increased integrated area of the molecular desorption peak and the surface area calculated from STM images. Surface defects cause a red shift in the photodissociation threshold of chlorobenzene and 3-chloropyridine, and it is suggested that the shift to lower photon energies is due to either excitation of a surface plasmon resonance, which is allowed on the rough surface but not the smooth, or a more localized excitation of the surface−adsorbate complex near defect sites. The photodissociation yield at higher photon

energies is increased on the rough surface as compared to the smooth for 3-chloropyridine and decreased for chlorobenzene. Classical electromagnetic theory suggests that the enhanced yield for 3-chloropyridine on a rough surface is due to a decrease in the quenching (or decay rate) when adsorbed on the rough surface compared to the smooth i.e., $\Gamma_R < \Gamma_S$, whereas the reduced yield for chlorobenzene is due to an increase in quenching (or the decay rate) when adsorbed on the rough, i.e., $\Gamma_R > \Gamma_S$. Differences in the molecular orientation of these molecules may be the cause of this behavior. The experimental and theoretical results suggest that enhancement in the photoyield and absorption cross sections will only occur for molecules of certain adsorbate orientations.

Acknowledgment is made to the donors of the Petroleum Research Fund, administered by the American Chemical Society, for partial support of this research. The authors also gratefully acknowledge the National Science Foundation (Grant CHE-9300808) for support of this research. K.B.M. thanks the General Electric Foundation for support in the form of a General Electric Graduate Fellowship.

References and Notes

(1) Wandelt, K. *Surf. Sci.* **1991**, *251/252*, 387.
(2) Behm, R. J.; Holser, W. In *Springer Series in Surface Science: Chemistry and Physics of Solid Surfaces*; Springer-Verlag: New York, 1986; Vol. 6.
(3) Somorjai, G. A. *Introduction To Surface Chemistry and Catalysis*; Wiley-Interscience: New York, 1994.
(4) Jenks, C. J.; Paul, A.; Smoliar, A.; Bent, B. E. *J. Phys. Chem.* **1994**, *98*, 572.
(5) Van Duyne, R. P. In *Chemical and Biochemical Applications of Lasers*; Moore, C. B., Ed.; Academic: New York, 1979; Vol. 4.
(6) Chen, C. K.; de Castro, A. R. B.; Shen, Y. R. *Phys. Rev. Lett.* **1981**, *46*, 145.
(7) Nitzan, A.; Brus, L. E. *J. Chem. Phys.* **1981**, *75*, 2205.
(8) Gersten, J.; Nitzan, A. *J. Chem. Phys.* **1981**, *75*, 1139.
(9) Das, P. C.; Puri, A.; George, T. F. *J. Chem. Phys.* **1990**, *93*, 9106.
(10) Craighead, H. G.; Glass, A. M. *Opt. Lett.* **1981**, *6*, 248.
(11) Garoff, S.; Weitz, D. A.; Gramila, T. J.; Hanson, C. D. *Opt. Lett.* **1981**, *6*, 245.
(12) Goncher, G. M.; Parsons, C. A.; Harris, C. B. *J. Phys. Chem.* **1984**, *88*, 4200.
(13) Wolkow, R. A.; Moskovitz, M. *J. Chem. Phys.* **1987**, *87*, 5858.
(14) Franzke, D.; Wokaun, A. *J. Phys. Chem.* **1992**, *96*, 6377.
(15) Garoff, S.; Weitz, D. A.; Alvarez, M. S. *Chem. Phys. Lett.* **1982**, *93*, 283.
(16) Suh, J. S.; Moskovitz, M.; Shakhesemampour, J. *J. Phys. Chem.* **1993**, *97*, 1678.
(17) Chen, C. J.; Osgood, R. M. *Phys. Rev. Lett.* **1983**, *50*, 1705.
(18) Henglein, A. *J. Phys. Chem.* **1993**, *97*, 5457.
(19) Henglein, A.; Lindig, B.; Westerhausen, J. *J. Phys. Chem.* **1981**, *85*, 1627.
(20) Michaelis, M.; Henglein, A. *J. Phys. Chem.* **1992**, *96*, 4719.
(21) Zhou, X.-L.; Zhu, X. Y.; White, J. M. *Surf. Sci. Rep.* **1991**, *13*, 73 and references therein.
(22) Myli, K. B.; Grassian, V. H. *J. Phys. Chem.* **1994**, *98*, 6237.
(23) Messinger, B. J.; Raben, K. U.; Chang, R. K.; Barber, P. W. *Phys. Rev. B* **1991**, *24*, 649.
(24) Redhead, P. A. *Vacuum* **1962**, *12*, 203.
(25) The adsorption temperature and the molecular desorption temperatures are approximately 10 K lower than those reported in a preliminary report of this work (ref 22). The temperatures quoted here reflect a more accurate reading of the thermocouple output at lower temperatures.
(26) Habenschaden, E.; Kuppers, J. *Surf. Sci.* **1984**, *138*, L147.
(27) The heat of sublimation for chlorobenzene and pyrazine was calculated to be 51 and 56 kJ, respectively, from known thermodynamic values.
(28) Avouris, P.; Demuth, J. E. *J. Chem. Phys.* **1981**, *75*, 4783.
(29) Demuth, J. E.; Christmann, K.; Sandra, P. N. *Chem. Phys. Lett.* **1980**, *76*, 201.
(30) Demuth, J. E.; Sanda, P. N.; Warlaumont, J. M.; Tsang, J. C.; Chritmann, K. In *Vibrations at Surfaces*; Plenum Press: New York, 1982.
(31) Song, Y.; Gardner, P.; Conrad, H.; Bradshaw, A. M.; White, J. M. *Surf. Sci.* **1991**, *248*, L279.
(32) Zhou, X.-L.; White, J. M. *J. Chem. Phys.* **1990**, *92*, 5612.
(33) McGee, K. C.; Grassian, V. H. Unpublished data.
(34) *The Sadtler Standard Spectra*; Sadtler Research Laboratories, 1980.
(35) Sass, J. K.; Laucht, H.; Kliewer, K. L. *Phys. Rev. Lett.* **1975**, *35*, 1461.
(36) Castor, M. E.; White, J. M. *J. Chem. Phys.* **1991**, *95*, 6057.
(37) The polarizability of C_6H_5Cl is found in the *CRC Handbook of Chemistry and Physics*, 72nd ed., CRC Press: Boca Raton, FL, 1991. The polarizability of 3-chloropyridine was estimated using values for similar compounds.
(38) Arias, J.; Aravind, P. K.; Metiu, H. *Chem. Phys. Lett.* **1982**, *85*, 404.
(39) Fischer, S.; Schneider, S. *Chem. Phys. Lett.* **1971**, *10*, 392.
(40) Prais, M. G.; Heller, D. F.; Freed, K. F. *Chem. Phys.* **1974**, *6*, 331.
(41) Hornburger, H.; Brand, J. *Chem. Phys. Lett.* **1982**, *88*, 153.
(42) Sun, Z.-J.; White, J. M. *J. Vac. Sci. Technol. A* **1993**, *11*, 1921.

JP951790F